Electronic Supplementary Material (ESI) for Nanoscale.
This journal is © The Royal Society of Chemistry 2015

Supplementary Information: Dirac point movement and topological phase transition in patterned graphene

Marc Dvorak and Zhigang Wu*

Department of Physics, Colorado School of Mines, Golden, CO

E-mail: zhiwu@mines.edu

Virtual Crystal Approximation

In the virtual crystal approximation (VCA), an effective 2×2 tight-binding (TB) Hamiltonian is constructed for a defected graphene supercell. First, on-site energies and hopping parameters are calculated for all N atoms in the supercell. These quantities are then averaged separately over graphene's A and B sublattices. After averaging, these values are inserted into the familiar TB Hamiltonian on a honeycomb lattice. We limit our discussion to on-site energies and nearest neighbor hopping only. The on-site energy of the i^{th} atom in the supercell - a C atom or a defect - is given by

$$E_i = \langle \phi_i(\mathbf{r} - \mathbf{R}_i) | H | \phi_i(\mathbf{r} - \mathbf{R}_i) \rangle . \tag{1}$$

Supercell averages give on-site energies for A and B sublattices. On-site energies are averaged over A- and B-sublattice separately. Each sublattice contains $N/2$ atoms in the supercell.

*To whom correspondence should be addressed

$$
\begin{aligned}
E_{\mathrm{A}} &= \frac{1}{N/2}\sum_{i\in \mathrm{A}}^{N/2} E_i \\
E_{\mathrm{B}} &= \frac{1}{N/2}\sum_{i\in \mathrm{B}}^{N/2} E_i
\end{aligned} \tag{2}
$$

There are three nearest neighbor vectors δ_j. The hopping parameter for the i^{th} atom in the j^{th} nearest neighbor direction is

$$
t_{ji} = \langle \phi_{i+\delta_j}(\mathbf{r} - (\mathbf{R}_i + \delta_j)) | H | \phi_i(\mathbf{r} - \mathbf{R}_i) \rangle \,. \tag{3}
$$

The three distinct VCA hopping parameters t_j for each direction δ_j are calculated as

$$
t_j = \frac{1}{N/2}\sum_{i\in \mathrm{A}}^{N/2}\sum_{k=j} t_{ik}. \tag{4}
$$

Here, there are three distinct hopping parameters t_j. The sum over $k = j$ serves to pick out the proper j^{th} direction from all hopping parameters t_{ik}. The sum over i averages the hopping parameters over the $N/2$ atoms in the A sublattice. We only sum over the A sublattice to avoid double counting each hopping integral ($i \to k$ and $k \to i$). With the VCA hopping parameters, the locations of the Dirac points are at the roots of the following equation.

$$
f(\mathbf{k}) = t_1 e^{i\mathbf{k}\cdot\delta_1} + t_2 e^{i\mathbf{k}\cdot\delta_2} + t_3 e^{i\mathbf{k}\cdot\delta_3} = 0 \tag{5}
$$

Dirac point movement

On the isotropic honeycomb lattice, the Dirac points ($\mathbf{D}_\pm$) exist at the corners of the Brillouin zone ($\mathbf{K}$ and $\mathbf{K}'$), just as in pristine graphene. On the anisotropic honeycomb lattice, the Dirac points move away from $\mathbf{K}$ and $\mathbf{K}'$. When two of the hopping parameters are equal, $t_1 = t_2 \neq t_3$, the

movement of the Dirac point is in only one direction.[1]

$$\mathbf{D}_{\pm} = \left(\frac{2}{a} \arccos\left(-\frac{t_3}{2t_1} \right), 0 \right) \tag{6}$$

When all three hopping parameters are different, the Dirac points are located at[2]

$$\begin{aligned} D_{x,\pm} &= \pm\frac{2}{a} \arccos\left(-\sqrt{\frac{t_3^2 - (t_2 - t_1)^2}{4t_1 t_2}} \right) \\ D_{y,\pm} &= \pm\frac{2}{\sqrt{3}a} \mathrm{sgn}(t_1 - t_2) \arccos\left(\frac{t_1 + t_2}{t_3} \sqrt{\frac{t_3^2 - (t_2 - t_1)^2}{4t_1 t_2}} \right). \end{aligned} \tag{7}$$

Consider generic VCA hopping parameters given by

$$\begin{aligned} t_1 &= (1 - f_d) t_{\mathrm{CC}} + f_d t_1' \\ t_2 &= (1 - f_d) t_{\mathrm{CC}} + f_d t_2' \\ t_3 &= (1 - f_d) t_{\mathrm{CC}} + f_d t_3'. \end{aligned} \tag{8}$$

Here, t_i' represents the hopping parameter in the i^{th} direction averaged *only* for the defect atoms. By considering the surrounding C atoms, the t_i' enter the VCA with the weight of f_d; ordinary C-C hopping enters with the weight $(1 - f_d)$.

After inserting Eq. 8 into Eq. 7, the Dirac points are located at

$$\begin{aligned} D_{x,\pm} &= \pm\frac{2}{a} \arccos\left(-\frac{1}{2} \sqrt{\frac{(f_d t_3' + (1 - f_d) t_{\mathrm{CC}})^2 - (f_d t_2' - f_d t_1')^2}{(f_d t_1' + (1 - f_d) t_{\mathrm{CC}})(f_d t_2' + (1 - f_d) t_{\mathrm{CC}})}} \right) \\ D_{y,\pm} &= \pm\frac{2}{\sqrt{3}a} \mathrm{sgn}(f_d t_1' - f_d t_2') \\ &\quad \arccos\left(\frac{(f_d t_1' + f_d t_2' + 2(1 - f_d) t_{\mathrm{CC}}) \sqrt{\frac{-(-f_d t_1' + f_d t_2')^2 + (f_d t_3' + (1 - f_d) t_{\mathrm{CC}})^2}{(f_d t_1' + (1 - f_d) t_{\mathrm{CC}})(f_d t_2' + (1 - f_d) t_{\mathrm{CC}})}}}{2(f_d t_3' + (1 - f_d) t_{\mathrm{CC}})} \right) \end{aligned} \tag{9}$$

A few test cases illustrate how the Dirac points move in our VCA-TB approximation. When

$t'_1 = t'_2 = t'_3$, the Dirac points remain at their original locations,

$$\mathbf{D}_\pm = \pm\left(\frac{4\pi}{3a}, 0\right). \tag{10}$$

When $t'_1 = t'_2 = t_{\rm CC}$ and $t'_3 = 2t_{\rm CC}$, the Dirac points are at

$$\mathbf{D}_\pm = \pm\left(\frac{2}{a}\arccos\left(\frac{-(1+f_d)}{2}\right), 0\right). \tag{11}$$

The case $t'_1 = t_{\rm CC}$, $t'_2 = 2t_{\rm CC}$, $t'_3 = 3t_{\rm CC}$ has Dirac points at

$$\begin{aligned} D_{x,\pm} &= \pm\frac{2}{a}\arccos\left(-\frac{1}{2}\sqrt{1+3f_d}\right) \\ D_{y,\pm} &= \pm\frac{-2}{\sqrt{3}a}\mathrm{sgn}(f_d t_{\rm CC})\arccos\left(\frac{(2+f_d)\sqrt{1+3f_d}}{2+4f_d}\right) \end{aligned} \tag{12}$$

The defect averaged hopping parameters t'_i depend on the local defect geometry. For the BN defect shown in Fig. 1, the t_i are

$$\begin{aligned} t'_1 &= (t_{\rm CC} + t_{\rm BC} + t_{\rm NC})/3 \\ t'_2 &= (7t_{\rm CC} + t_{\rm BC} + t_{\rm NC} + 3t_{\rm BN})/12 \\ t'_3 &= (5t_{\rm CC} + t_{\rm BN} + 3t_{\rm BC} + 3t_{\rm NC})/12. \end{aligned} \tag{13}$$

The two supercells in Fig. 1 have identical defects and, hence, identical t'_i. These two structures demonstrate a practical realization to test the parameterization of the hopping parameters in Eq. 8 and the movemement of Dirac points based on Eq. 9.

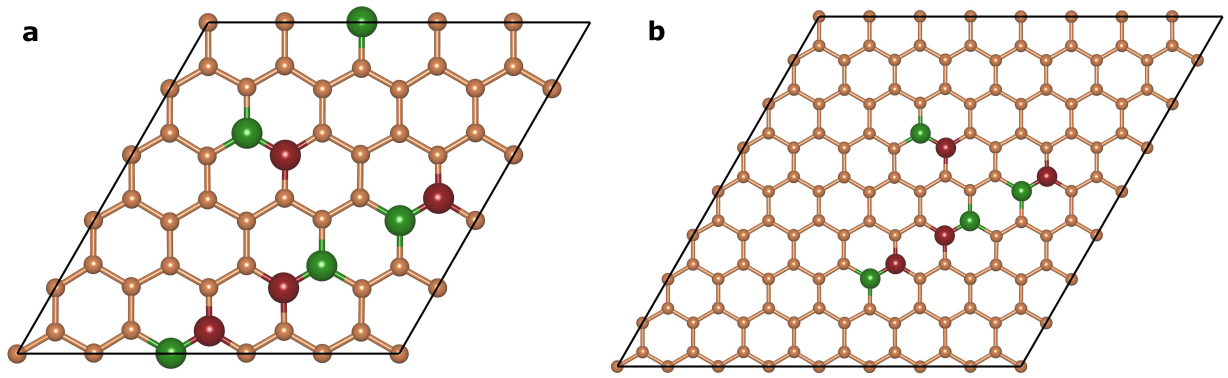

Figure 1: **BN doped defect with $t_1' \neq t_2' \neq t_3'$.**

Intervalley Scattering

Consider Dirac points at the positions in reciprocal space $\mathbf{D}$ and $\mathbf{D}' = -\mathbf{D}$. The scattering matrix element between eigenstates of pristine graphene is given by[3]

$$\langle s, \mathbf{k}| U(\mathbf{r}) |s', \mathbf{k}'\rangle = \sum_{\mathbf{G}} \frac{1}{2}(1 + ss' e^{-i\theta_{\mathbf{k},\mathbf{k}'}}) U(\mathbf{G}) \delta_{\mathbf{k}', \mathbf{k}-\mathbf{G}} \tag{14}$$

where $\theta_{\mathbf{k},\mathbf{k}'}$ is the angle in reciprocal space between the scattered states.

If the impurity potential $U(\mathbf{r})$ has a range much larger than the carbon-carbon distance in graphene, intervalley scattering does not occur between $\mathbf{D}$ and $\mathbf{D}'$ and a band gap can not open.[3,4] However, if the perturbing potential has oscillations on the order of the carbon-carbon distance, $U(\mathbf{G})$ has significant contributions at large $|\mathbf{G}|$ - such as some $\mathbf{G}$ connecting $\mathbf{D}$ and $\mathbf{D}'$ - and band gap opening can occur. This is the case for structural modifications on graphene. Defects create a scattering potential somewhere between a slowly varying potential and a perfectly localized δ-function.

The intervalley scattering matrix element is nonzero only if $\mathbf{D}$ and $\mathbf{D}'$ can be connected by a reciprocal lattice vector. This can only occur if the Dirac points are at certain high symmetry locations in the Brillouin zone. The Kroenecker-δ in Eq. 14 is satisfied when the Dirac points drift

to the zone center (Γ) or the points $\mathbf{M}_i = \mathbf{G}_i/2$. When $\mathbf{D} = \mathbf{D}' = \Gamma \mod \mathbf{G}_i$,

$$\mathbf{D} - \mathbf{D}' = 2\mathbf{G}_i. \tag{15}$$

When $\mathbf{D} = \mathbf{M} = \mathbf{G}_i/2$ and $\mathbf{D}' = -\mathbf{M} = -\mathbf{G}_i/2$,

$$\mathbf{D} - \mathbf{D}' = \mathbf{G}_i. \tag{16}$$

BN Doping

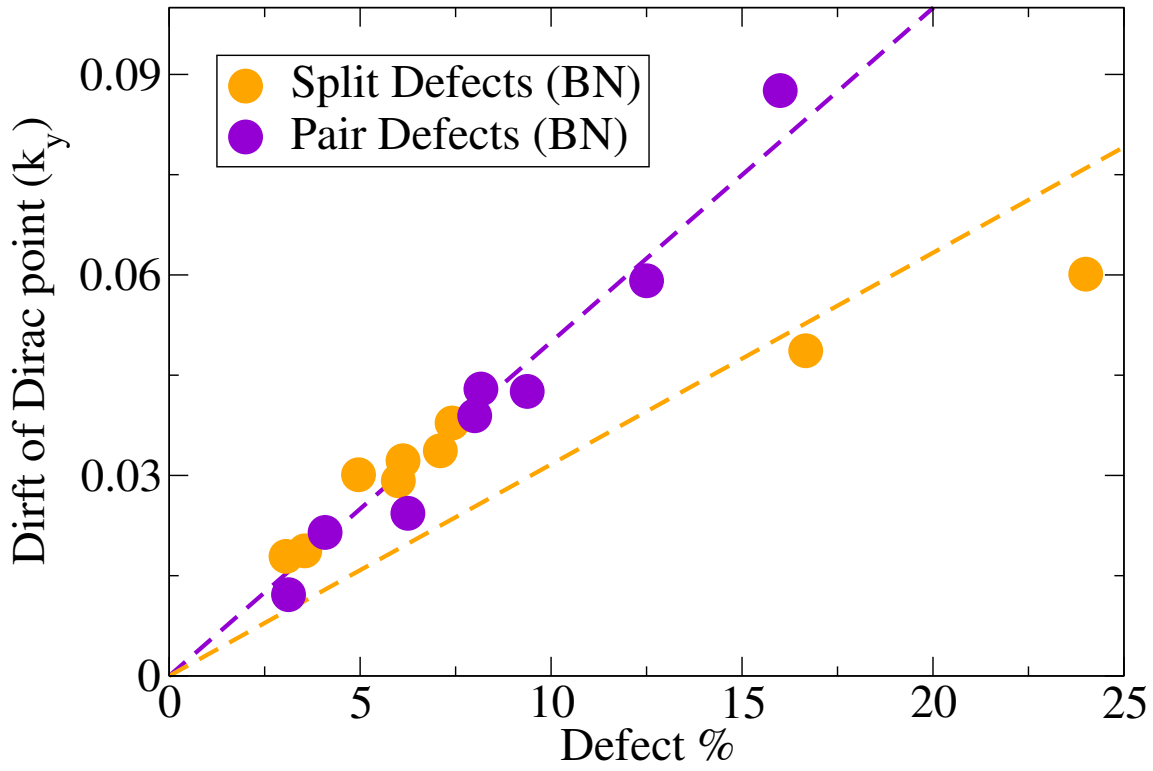

Figure 2: **Drift of Dirac points depends on defect fraction** The drift of the Dirac point in BN doped graphene increases with defect fraction. Plotted values are the magnitude of the drift. For split defects, the drift is in the $-k_y$ direction, and for pair defects, the drift is in the $+k_y$ direction. Overall balance in on-site energies between A and B sublattices is achieved by switching B and N dopants between sublattices for different defects. Hence, each BN doped supercell must have an even number of defects. The ratio of the fitted slopes is 0.63.

Brillouin zones

The Brillouin zone, high symmetry points, and band structure path of the 5×5 graphene supercell used in the text are shown below. All plotted band structures belong to hexagonal supercells with the same shape. Therefore, all Brillouin zones have the same shape and high symmetry points and differ only in size. Hexagonal supercells are particularly convenient for tracking the movement of Dirac points in the case of $t_1 = t_2 \neq t_3$ because the Dirac points move in a direction that is along the band structure path shown here. For an arbitrarily shaped supercell, the Dirac points may move off of the band structure path and not be visibile in the band structure plot.

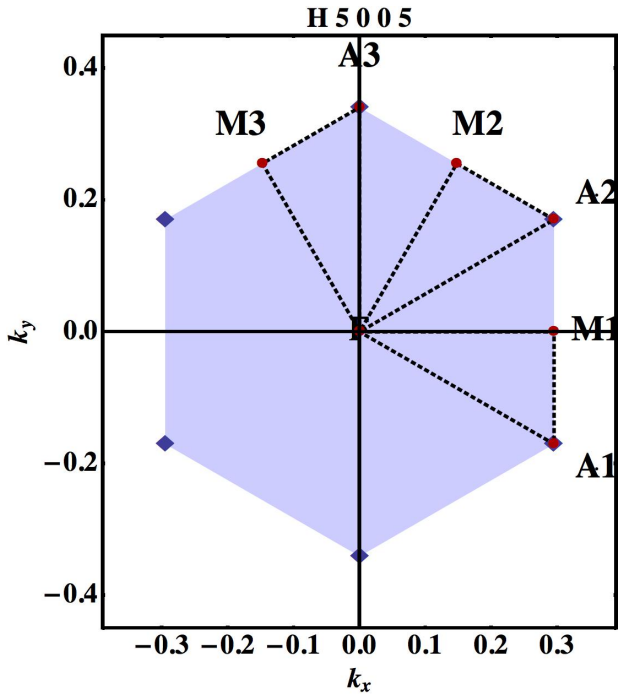

Figure 3: **BZ of** 5×5 **graphene supercell**.

References

1. Pereira, V. M.; Castro Neto, A. H.; Peres, N. M. R. Tight-binding approach to uniaxial strain in graphene. *Phys. Rev. B* **2009**, *80*, 045401.

2. Wunsch, B.; Guinea, F.; Sols, F. Dirac-point engineering and topological phase transitions in honeycomb optical lattices. *New J. Phys.* **2008**, *10*, 103027.

3. Park, C.-H.; Yang, L.; Son, Y.-W.; Cohen, M. L.; Louie, S. G. Anisotropic behaviours of massless Dirac fermions in graphene under periodic potentials. *Nature Phys.* **2008**, *4*, 213–217.

4. Ando, T.; Nakanishi, T. Impurity Scattering in Carbon Nanotubes - Absence of Back Scattering. *J. Phys. Soc. Jap.* **1998**, *67*, 1704–1713.